

## **Electronic supplementary information for**

### **The electron injection rate in CdSe quantum dots sensitized solar cells: From bifunctional linker and zinc oxide morphology**

Wei-Lu Ding,<sup>a</sup> Xing-Liang Peng,<sup>a</sup> Zhu-Zhu Sun,<sup>b</sup> and Ze-Sheng Li<sup>\*a</sup>

<sup>a</sup> Beijing Key Laboratory of Cluster Science of Ministry of Education, Key Laboratory of Photoelectronic/Electrophotonic Conversion Materials, School of Chemistry and chemical engineering, Beijing Institute of Technology, Beijing 100081, China

<sup>b</sup> Energy-Saving Building Materials Innovative Collaboration Center of Henan Province, Xinyang Normal University, Xinyang, 464000, China

**Corresponding Author:** zeshengli@bit.edu.cn (Z.-S. Li)

## CONTENTS

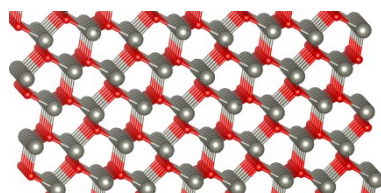
<b>Fig. S1</b> The model of ZnO substrate.....	S3-4
<b>Fig. S2</b> The relaxed structures for bare (CdSe) <sub>33</sub> performed by varied functionals and basis sets in different programs. ....	S5
<b>Fig. S3</b> The simulated absorption spectra of bare (CdSe) <sub>33</sub> by varied levels.....	S6
<b>Fig. S4</b> The relaxed structures of ZnO/L1/CdSe QDs heterogeneous.....	S7
<b>Fig. S5</b> The relaxed structures of ZnO/L2/CdSe QDs heterogeneous.....	S8
<b>Fig. S6</b> The relaxed structures of ZnO/L3/CdSe QDs heterogeneous.....	S9
<b>Fig. S7</b> The relaxed structures of ZnO/L4/CdSe QDs heterogeneous.....	S10
<b>Fig. S8</b> The simulated absorption spectra of linker/QDs before tethering on ZnO.....	S11
<b>Fig. S9</b> Molecular weight of linker and QDs involved in the associated orbitals during excitation for linker/QDs complexes.....	S12
<b>Fig. S10</b> The main contributions involved in the maximum absorption peak ( $\lambda_{\max}$ ) of linker/QDs complex in C <sub>2</sub> H <sub>5</sub> OH solution before tethering on ZnO substrate.....	S13-14
<b>Fig. S11</b> The simulated absorption spectra of linker/QDs complexes after tethering on ZnO.....	S15
<b>Table S1</b> The adsorption energy of L1-L4 on CdSe QDs.....	S16
<b>Table S2</b> The adsorption energy of L1-L4 on varied ZnO substrates.....	S16
<b>Table S3</b> The parameters related to the maximum absorption peak of linker/QDs complex...	S16
<b>Discussions of optical properties.....</b>	S17-20

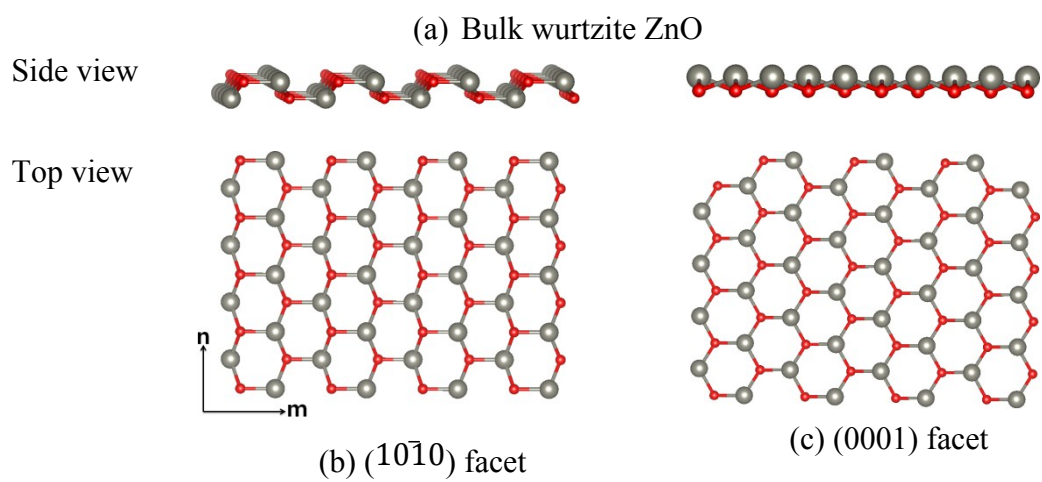
## The model of ZnO substrate

For bulk wurtzite ZnO (Fig. S1 (a)), it has four principal low-index surfaces, i.e., two nonpolar facets,  $(10\bar{1}0)$  and  $(11\bar{2}0)$ , and two polar surfaces,  $(0001)$ -Zn and  $(000\bar{1})$ -O. The two nonpolar surfaces consist of equal numbers of cations and anions in each layer (the example of  $(10\bar{1}0)$  facet has been shown in Fig. S1 (b)), and the two polar surfaces consist of monolayers of cations and anions alternating along the c-axis (the example of  $(0001)$  facet has been shown in Fig. S1 (c)).

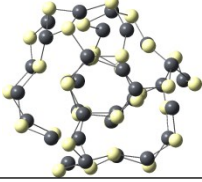
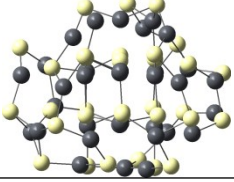
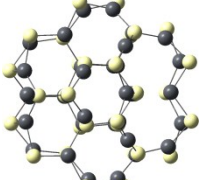
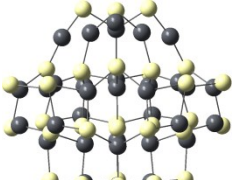
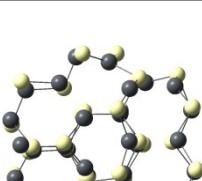
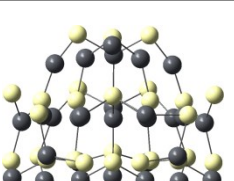
In this work, we only consider the variation in morphology based on the nonpolar  $(10\bar{1}0)$  facet because it contains both acid and basic sites (Zn and O atoms), which in principle favors the dissociation of weak acids on it and enhances its reactivity against such molecules.<sup>1,2</sup>

The employed ZnO nanoparticles (NPs) were constructed by clipping a wurtzite slab to show the  $(10\bar{1}0)$  surface, where it is without unsaturated atoms or groups at the boundary, and is an almost-square four-layer slab. For ZnO nanowires (NWs), the hexagonal prisms with  $(0001)$ -orientated axes enclosed by six facets belonging to the  $(10\bar{1}0)$  surface were constructed. As for single-walled ZnO nanotubes, namely (6,6)-NTs-A and (9,0)-NTs-Z, they are constructed by rolling a  $(10\bar{1}0)$  sheet along the m or n direction labeled in Fig. S1 (b).<sup>3</sup>





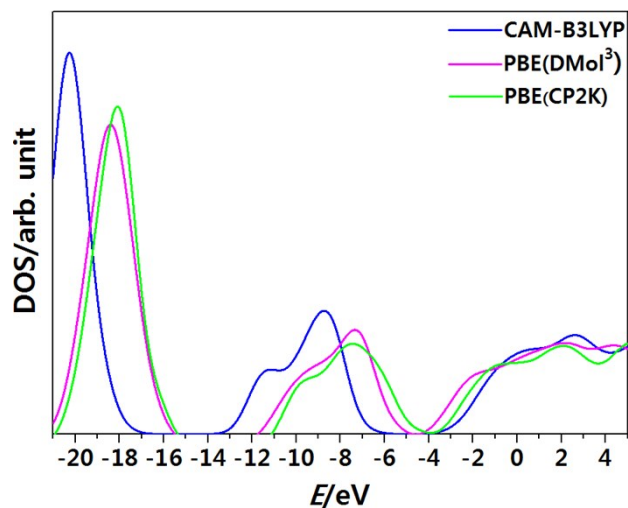
**Fig. S1** Schematic representation of the (a) bulk wurtzite ZnO, (b) the  $(10\bar{1}0)$  facet, and (c) the  $(0001)$  facet (Light gray = Zn, red = O atoms).

Functionals	Top view	Side view
CAM-B3LYP <sup>a</sup>		
PBE <sup>b</sup>		
PBE <sup>c</sup>		

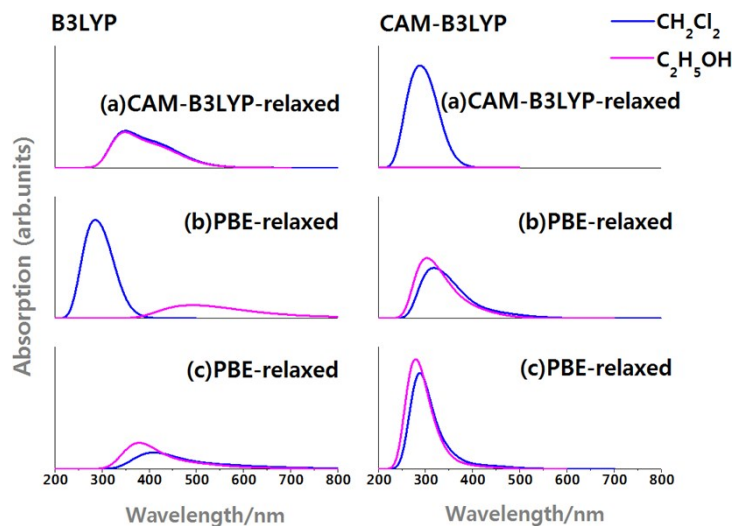
<sup>a</sup>The start point relaxed by Gaussian 09 D.01 program (LANL2DZ basis set).

<sup>b</sup>The start point relaxed by DMol<sup>3</sup> package in Materials Studio 8.0 (double numeric quality basis set with polarization functions (DNP)).

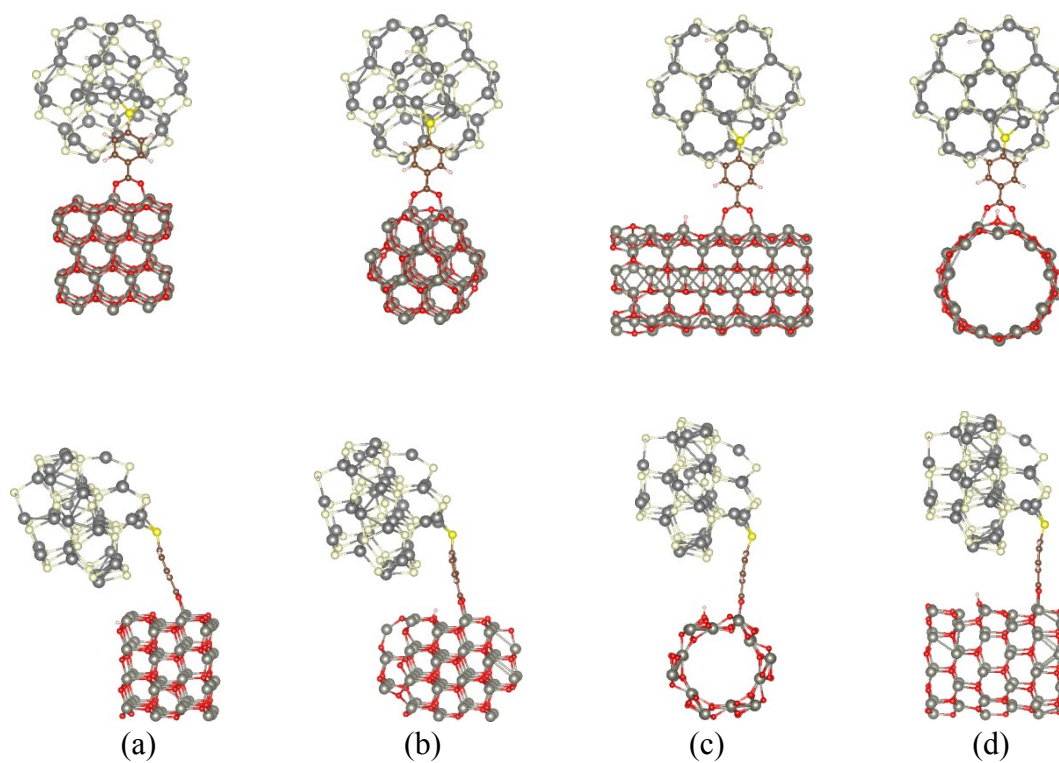
<sup>c</sup>The start point relaxed by CP2K/QUICKSTEP program (hybrid Gaussian and plane wave basis set).



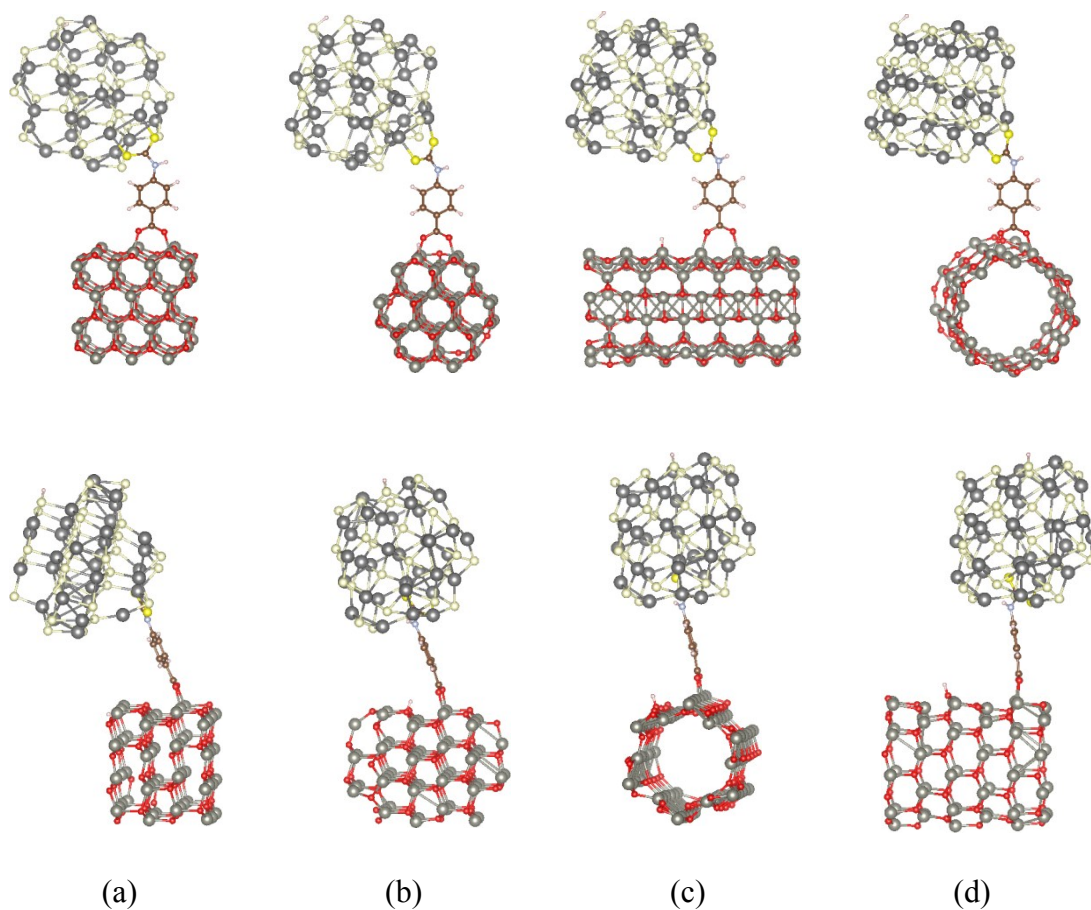
**Fig. S2** The relaxed structures for bare  $(\text{CdSe})_{33}$  performed by varied functionals and basis sets as implanted in the different programs.



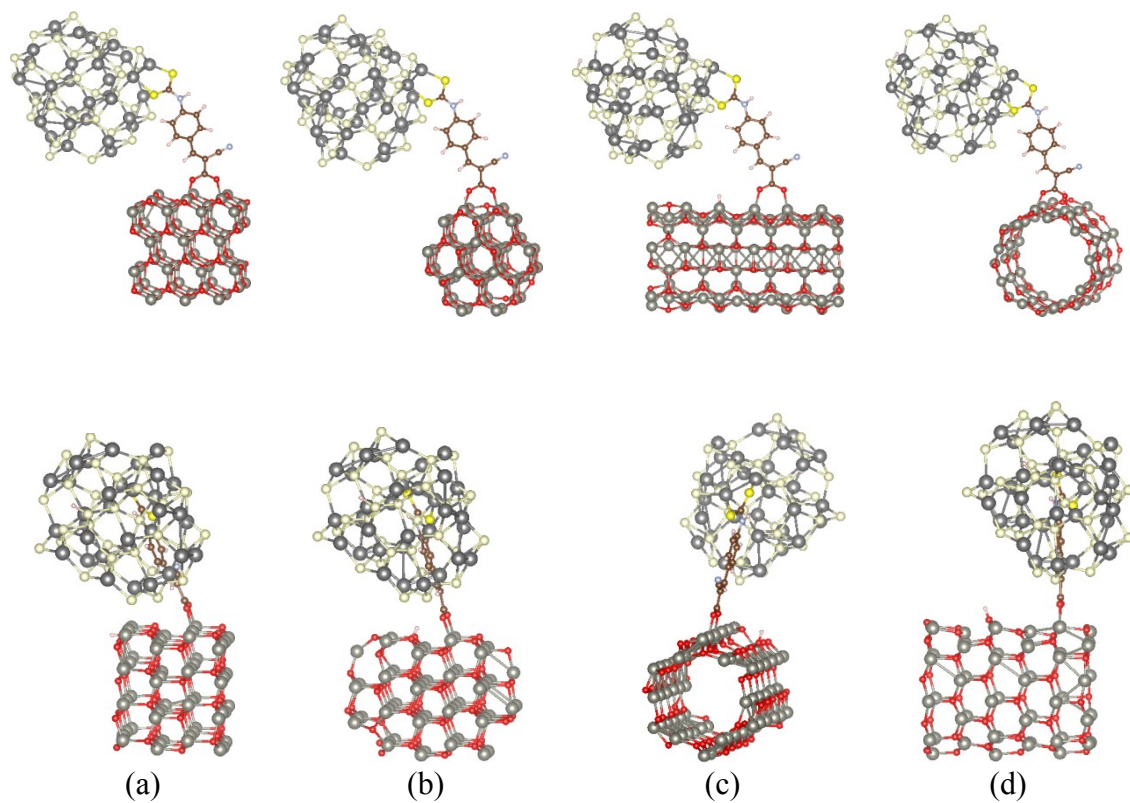
**Fig. S3** The simulated absorption spectra of bare  $(\text{CdSe})_{33}$  by B3LYP (the left column) and CAM-B3LYP (the right column) functionals on top of (a) CAM-B3LYP optimized structure (performed by Gaussian 09 D.01), (b) GGA-PBE optimized structure (performed by CP2K/QUICKSTEP version 2.6), and (c) GGA-PBE optimized structure (performed by DMol<sup>3</sup> as implanted in Materials Studio 8.0) (the blue and pink solid lines represents for the absorption spectra simulated in  $\text{CH}_2\text{Cl}_2$  and  $\text{C}_2\text{H}_5\text{OH}$  solution, respectively).



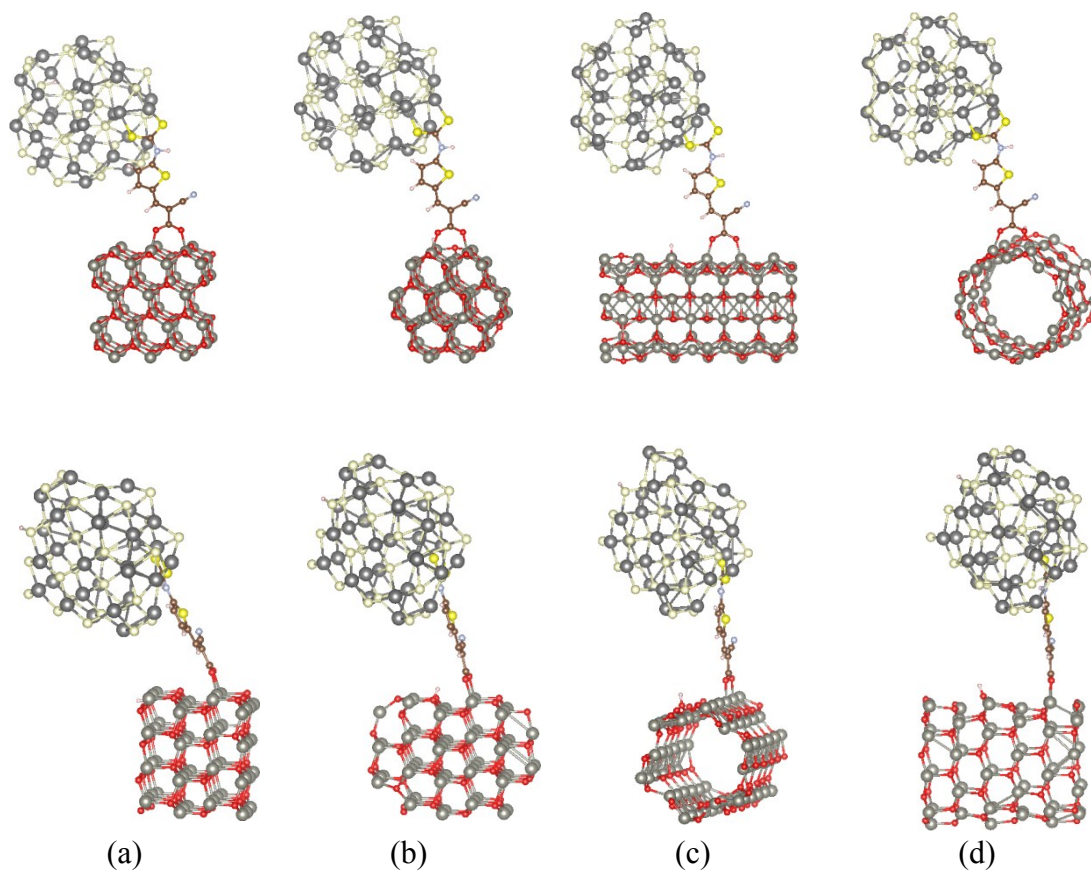
**Fig. S4** The side views of (a) L1/QDs@NPs, (b) L1/QDs@NWs, (c) L1/QDs@NTs-A, and (d) L1/QDs@NTs-Z, respectively.



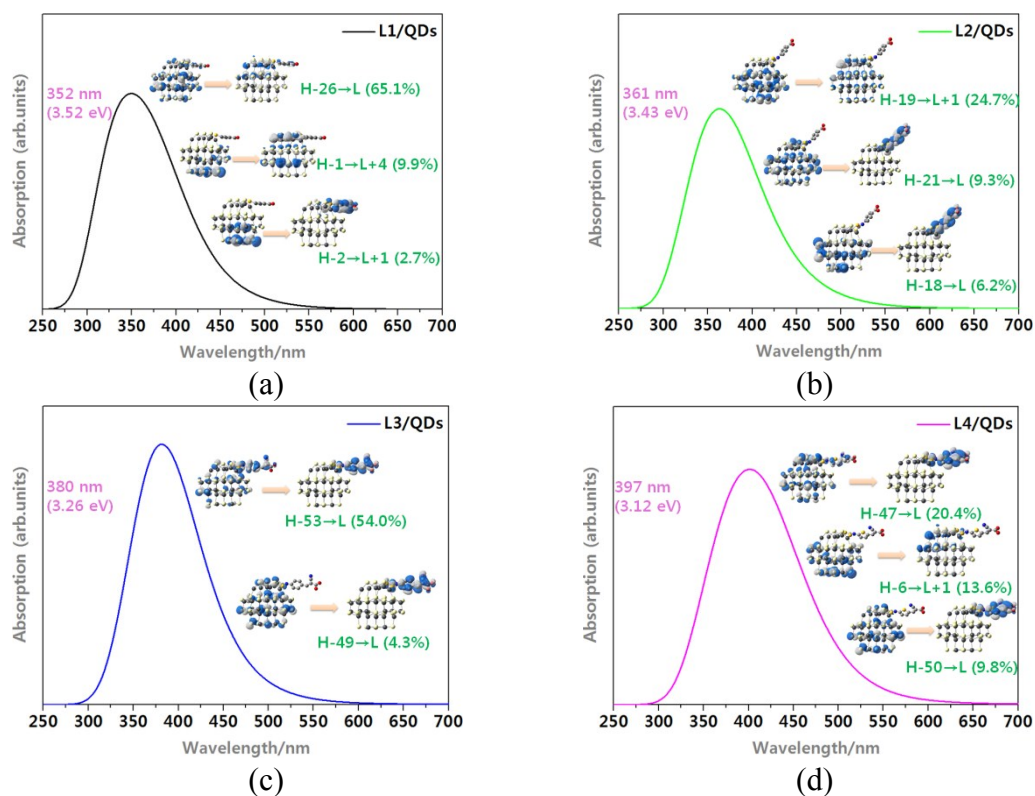
**Fig. S5** The side views of (a) L2/QDs@NPs, (b) L2/QDs@NWs, (c) L2/QDs@NTs-A, and (d) L2/QDs@NTs-Z, respectively.



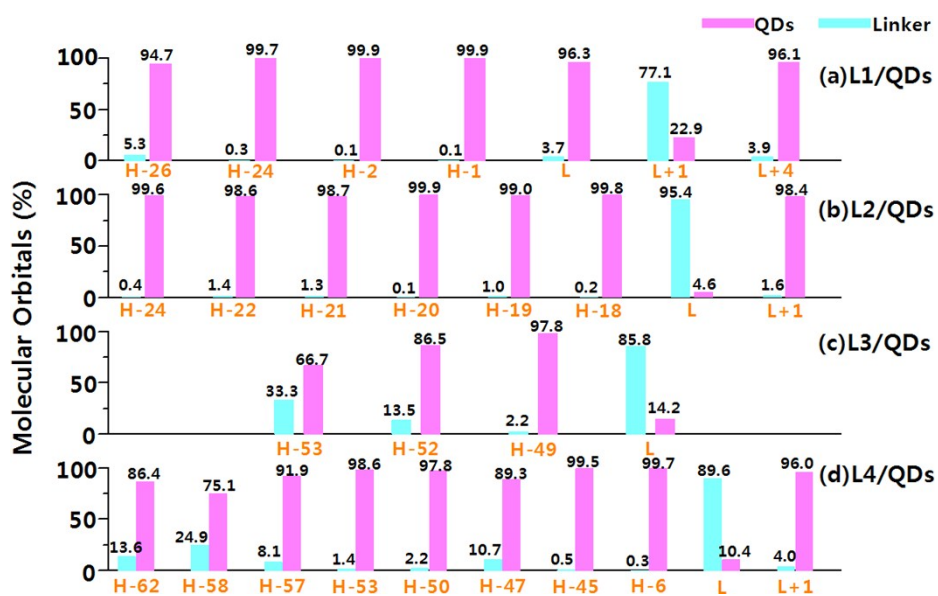
**Fig. S6** The side views of (a) L3/QDs@NPs, (b) L3/QDs@NWs, (c) L3/QDs@NTs-A, and (d) L3/QDs@NTs-Z, respectively.



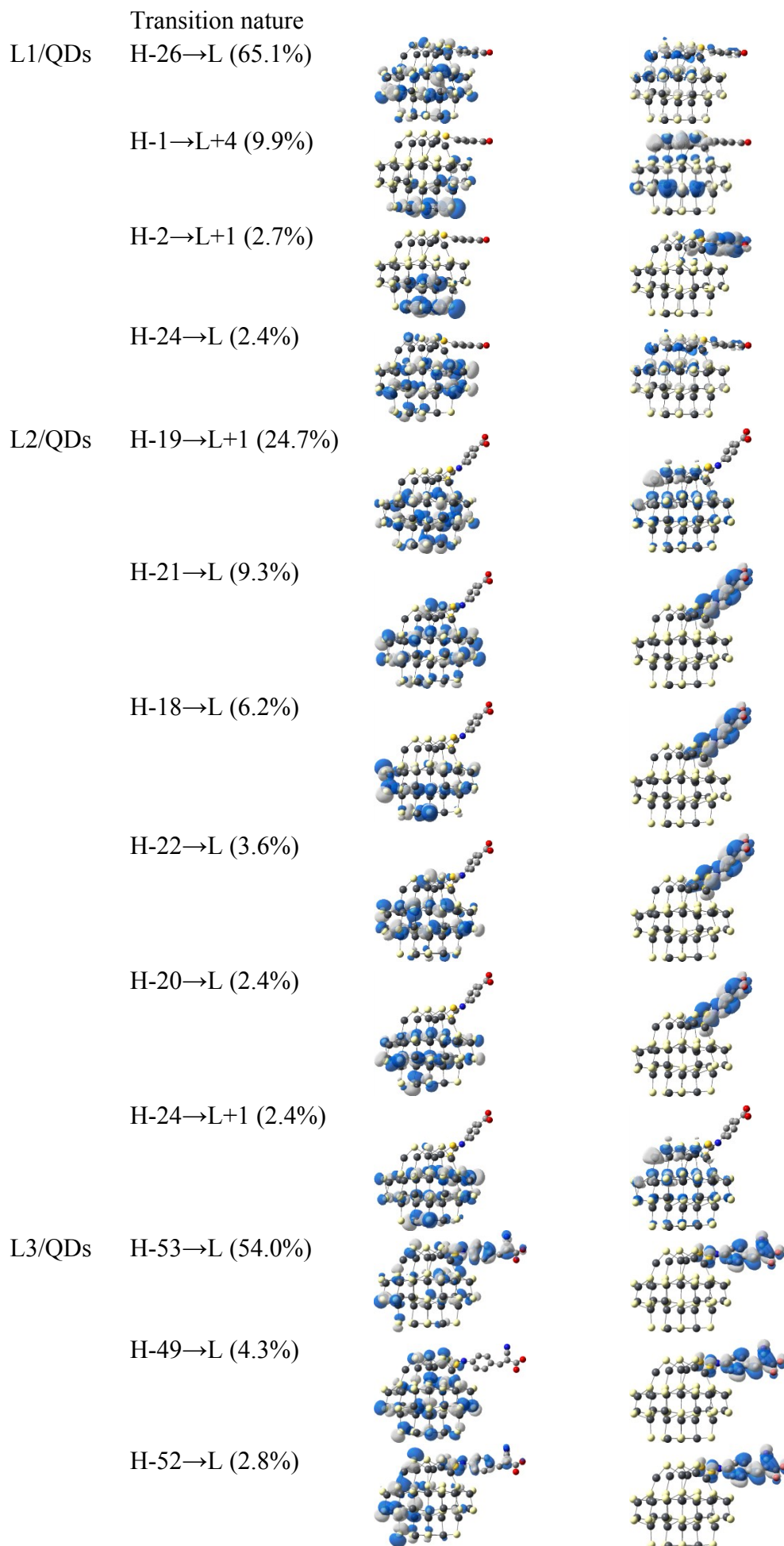
**Fig. S7** The side views of (a) L4/QDs@NPs, (b) L4/QDs@NWs, (c) L4/QDs@NTs-A, and (d) L4/QDs@NTs-Z, respectively.

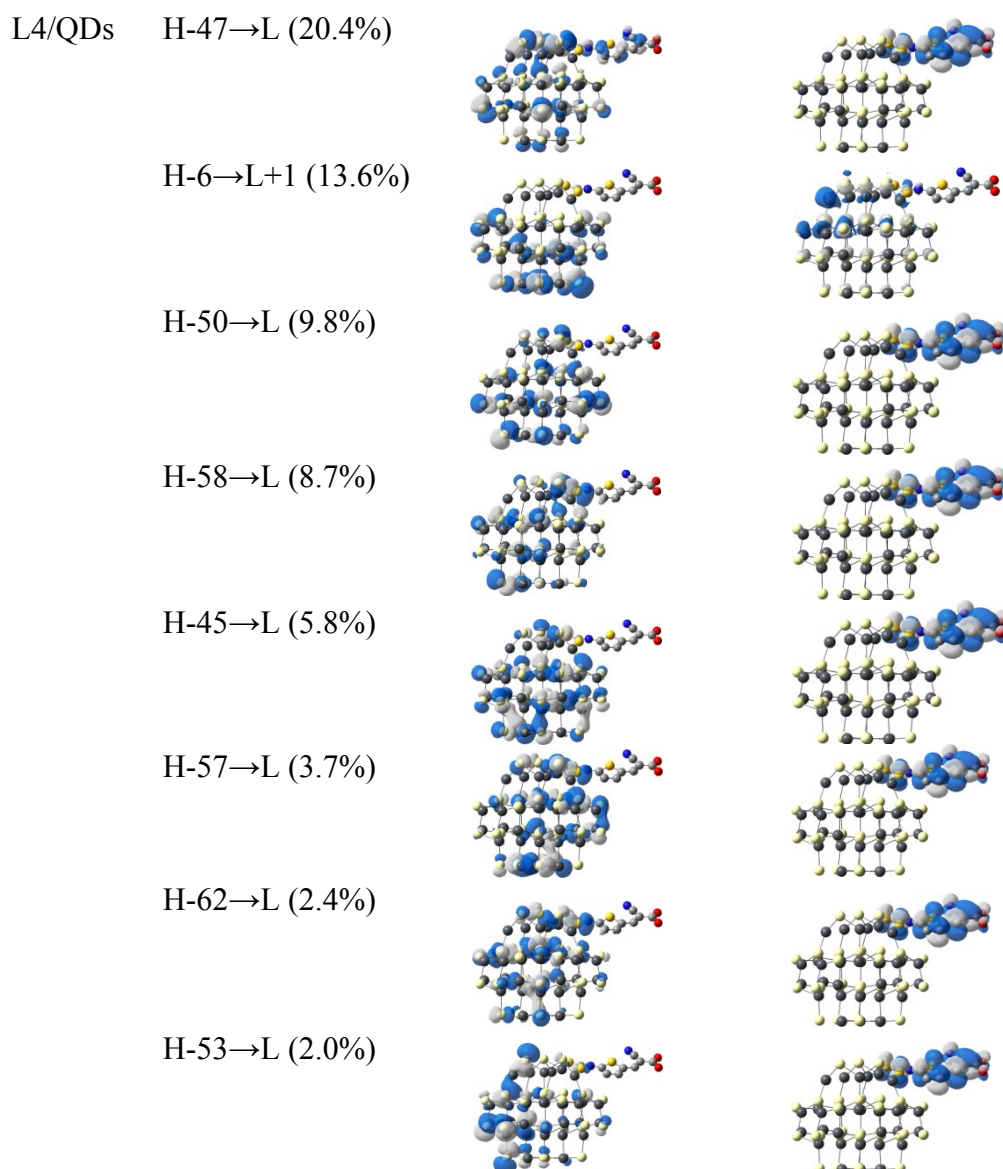


**Fig. S8** The simulated absorption spectra and the main contributions related to the maximum absorption peak ( $\lambda_{\max}$ ) of linker/QDs complex in  $C_2H_5OH$  solution before tethering on ZnO substrate: (a) L1/QDs, (b) L2/QDs, (c) L3/QDs, and (d) L4/QDs, respectively (more detailed transition characterization associated to the small contributions can be seen in Fig. S9).

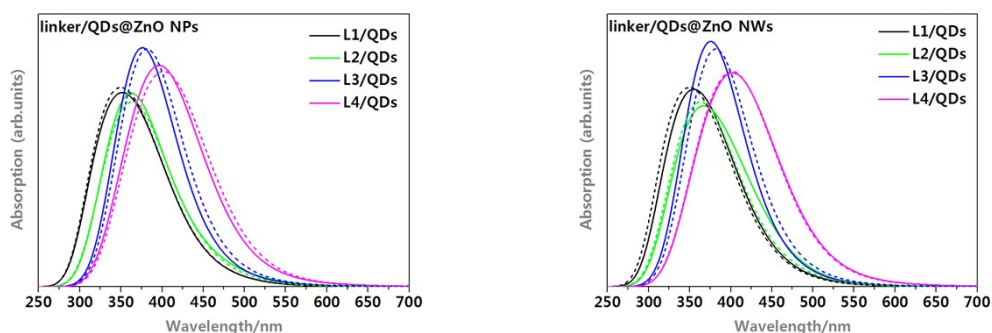


**Fig. S9** Molecular weight of linker and QDs involved in the associated orbitals during excitation for linker/QDs complexes: (a) L1/QDs, (b) L2/QDs, (c) L3/QDs, and (d) L4/QDs, respectively.





**Fig. S10** The main contributions involved in the maximum absorption peak ( $\lambda_{\max}$ ) of linker/QDs complex in  $C_2H_5OH$  solution before tethering on ZnO substrate: (a) L1/QDs, (b) L2/QDs, (c) L3/QDs, and (d) L4/QDs, respectively (plotted by Gaussian View, Isosurface=0.015 a.u).



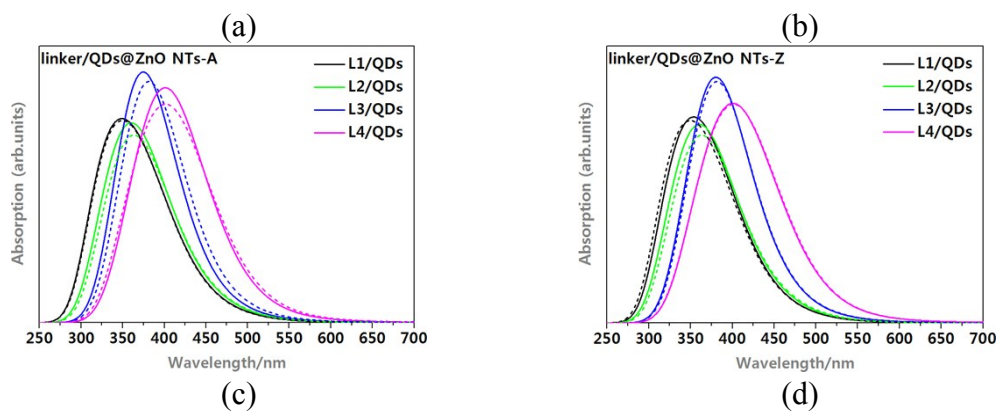


**Fig. S11** The simulated absorption spectra of linker/QDs complexes in  $C_2H_5OH$  solution after tethering on ZnO: (a) NPs, (b) NWs, (c) NTs-A, and (d) NTs-Z, respectively (the dot lines represent for the spectra before tethering).

**Table S1.** The adsorption energy ( $\Delta E_{\text{ads}}$ ) of L1-L4 on CdSe QDs (unit in eV).

	L1@QDs	L2@QDs	L3@QDs	L4@QDs
$\Delta E_{\text{ads}}$	-2.67	-3.37	-3.41	-3.30

**Table S2.** The adsorption energy ( $\Delta E_{\text{ads}}$ ) of L1-L4 on varied ZnO substrates (unit in eV).

	NPs	NWs	NTs-A	NTs-Z
L1	-3.30	-3.54	-3.71	-3.19
L2	-3.12	-3.40	-3.81	-3.30
L3	-3.54	-2.87	-3.92	-3.44
L4	-3.20	-3.30	-3.40	-3.67

**Table S3.** The parameters related to the maximum absorption peak ( $\lambda_{\text{max}}$ ) of linker/QDs complex.

		Transition nature		$\lambda_{\text{max}}/\text{nm}$	$\lambda_{\text{max}}/\text{nm}$ on ZnO
L1/QDs	S <sub>0</sub> -S <sub>37</sub>	H-26→L (65.1%)	H-1→L+4 (9.9%)	352	350 (-2) <sup>a</sup> , 354 (+2) <sup>b</sup> , 350 (-2) <sup>c</sup> , 353 (+1) <sup>d</sup>
		H-2→L+1 (2.7%)	H-24→L (2.4%)		
L2/QDs	S <sub>0</sub> -S <sub>45</sub>	H-19→L+1 (24.7%)	H-21→L (9.3%)	361	361 (0) <sup>a</sup> , 367 (+6) <sup>b</sup> , 361 (0) <sup>c</sup> , 360 (-1) <sup>d</sup>
		H-18→L (6.2%)	H-22→L (3.6%)		
		H-20→L (2.4%)	H-24→L+1 (2.4%)		
L3/QDs	S <sub>0</sub> -S <sub>65</sub>	H-53→L (54.0%)	H-49→L (4.3%)	380	374 (-6) <sup>a</sup> , 371 (-9) <sup>b</sup> , 373 (-7) <sup>c</sup> , 379 (-1) <sup>d</sup>
		H-52→L (2.8%)			
L4/QDs	S <sub>0</sub> -S <sub>57</sub>	H-47→L (20.4%)	H-6→L+1 (13.6%)	397	395 (-2) <sup>a</sup> , 398 (+1) <sup>b</sup> , 400 (+3) <sup>c</sup> , 397 (0) <sup>d</sup>
		H-50→L (9.8%)	H-58→L (8.7%)		
		H-45→L (5.8%)	H-57→L (3.6%)		
		H-62→L (2.4%)	H-53→L (2.0%)		

<sup>a</sup>The  $\lambda_{\text{max}}$  after tethering on NPs.<sup>b</sup>The  $\lambda_{\text{max}}$  after tethering on NWs.<sup>c</sup>The  $\lambda_{\text{max}}$  after tethering on NTs-A.<sup>d</sup>The  $\lambda_{\text{max}}$  after tethering on NTs-Z.<sup>e</sup>The data in parentheses represent for the shift of  $\lambda_{\text{max}}$  ( $\Delta\lambda_{\text{max}}$ ).

## Optical properties

### (i) Isolated linker/QDs

The optical properties of linker/QDs complexes have also been simulated for the aim of deep comprehension of the effect of energy level alignment on transition feature, all the simulated absorption spectra of complexes before tethering on ZnO have been depicted in Fig. S8. Notably, our estimated transition energy potentially leads to an observed discrepancy from experiment due to the diameters of the QDs synthesized by real experiment are estimated to be between 2.7 and 3.0 nm, while the diameters of our selected model are  $\sim 1.5$  nm. This potentially leads to a blue-shifted absorption peak because of quantum confinement effects. However, the goal of our calculations is not to reproduce the absolute energy scale of the spectrum, but rather to predict the spectrum on a relative energy scale, especially for the aim of assessment for novel designed L2, L3, and L4 capped QDs.

Clearly, the maximum absorption peak ( $\lambda_{\max}$ ) is red-shifted with variation of L1, L2, L3, and L4 in complexes (352, 361, 380, and 397 nm), and the  $\lambda_{\max}$  of L4/QDs presents the maximum shift ( $\Delta\lambda_{\max}$ ) by 45 nm compared to that of L1/QDs. To resolve the distinct  $\lambda_{\max}$  in these complexes, the transition nature and corresponding contribution imparted by different part in complex will be analyzed, and the molecular orbital percentage has been depicted in Fig. S9 intuitively.

For L1/QDs, the  $\lambda_{\max}$  arises from the  $S_0$ - $S_{37}$  transition, which mainly corresponds to the promotion of an electron from the  $H-26 \rightarrow L$  (65.1%), together with a small contributions from  $H-1 \rightarrow L+4$  (9.9%),  $H-2 \rightarrow L+1$  (2.7%), and  $H-24 \rightarrow L$  (2.4%). For

the main contribution, we find that the orbital of H-26 spreads over the complex (Fig. S8 (a)), and the amounts (the MO%) located on L1 and QDs are 5.3% and 94.7% separately (Fig. S9 (a)). After excited to the LUMO, it displays an apparent intramolecular charge transfer from L1 to QDs which is manifested by the increased and decreased electron distribution on QDs part (96.3%) and L1 (3.7%). Notably, although H-1→L+4, H-2→L+1, and H-24→L show a slight charge transfer from QDs to linker, their contributions to  $\lambda_{\max}$  are slight, thus confirming the leading intramolecular charge transfer of L1→QDs.

For L2/QDs, the  $\lambda_{\max}$  is induced by the transition from S<sub>0</sub>-S<sub>45</sub> state, which is mainly contributed from the H-19→L+1 (24.7%) combined with some slight items from the H-21→L (9.3%), H-18→L (6.2%), H-22→L (3.6%), H-24→L+1 (2.4%), and H-20→L (2.4%). Clearly from Fig. S8 (b), although all contributions present QDs→linker intramolecular charge transfer, it is subtle for the main contribution and pronounced for other small contributions.

Upon capping linker L3 on QDs, the transition correlated to the  $\lambda_{\max}$  (S<sub>0</sub>-S<sub>65</sub> state) features more pronounced QDs→linker charge transfer nature. From Table S3, the main contribution is H-53→L (54.0%), where the electron distribution varies from 66.7% vs. 33.3% for QDs vs. linker to 14.2% vs. 85.8% (Fig. S9 (c)) during the excitation. Simultaneously, some small contributions are detected containing H-49→L (4.3%) and H-52→L (2.8%), where H-49 and H-52 involve a considerable localization on linker part (MO%(L3) are 2.2 and 13.5%), dictating the participation

of linker in occupied states upon excitation. As a whole, all these contributions possess QDs→linker feature.

As for L4/QDs, more occupied orbitals involve in the transition. From Table S3, the main contribution arises from the H-47→L (20.4%), which shows a conspicuous charge transfer from QDs to linker (the MO% of QDs and linker related to this contribution change from 89.3% vs. 10.7% for QDs vs. linker to 10.4% vs. 89.6%). Meanwhile, a comparable contribution from H-6→L+1 (13.6%) features QDs→linker transfer can be detected. Besides these two large contributions, some other occupied orbitals positioned in the deeper region also present contributions, and some of them manifest a significant localization on linker part, e.g., H-62, H-58, and H-57 (MO% are 13.6, 24.9, and 8.1%, respectively).

These observations can be accounted by the fact aforementioned that the stronger/weaker electronic coupling in the virtual/occupied states varies to the weaker/stronger feature from L1/QDs to L4/QDs gradually. Hence, more empty orbitals in L1/QDs whereas more filled orbitals in L4/QDs participate in excitation. Moreover, the reason of the difference in the charge transfer direction in these complexes can be rationalized by the interfacial energy level alignment. Because the LUMO of L1-L4 shifts toward the LUMO(QDs) gradually, the  $\Delta G_e$  from L1, L2, L3, and L4 to QDs tends to decrease, thus, ensuring facile electron transfer from L1 to QDs. However, the downward LUMO level from L2 to L4 makes the electron delocalization from QDs to linker more easily compared to that in L1/QDs, therefore reflecting opposite transfer direction. For Interface-1 (type-I alignment), the excited

electrons should be delocalized on QDs not linker, and this is necessary for further electron injecting to ZnO efficiently, thus we confirm that L1 is more appropriate with regard to L2-L4.

**(ii) linker/QDs after tethering on ZnO**

As for the change tendency of  $\lambda_{\max}$  for all complexes after tethering on ZnO substrate, we observe a completely identical trend to the pictures before tethering (Fig. S11), i.e., L4/QDs > L3/QDs > L2/QDs > L1/QDs, respectively. Meanwhile, the  $\lambda_{\max}$  in all cases display a subtle shift ( $\Delta\lambda_{\max} < 10$  nm, see Table S3) with regard to the picture before attachment, indicating a negligible structural reconstruction and stable adsorption of QDs.

## References

1. N. H. Moreira, A. L. da Rosa and T. Frauenheim, *Appl. Phys. Lett.*, 2009, **94**, 193109.
2. A. Calzolari, A. Ruini and A. Catellani, *J. Am. Chem. Soc.*, 2011, **133**, 5893-5899.
3. S. Pal, B. Goswami and P. Sarkar, *J. Phys. Chem. C*, 2007, **111**, 1556-1559.